Reaction Mechanism of Chorismate Mutase Studied by the Combined Potentials of Quantum Mechanics and Molecular Mechanics

Yong S. Lee,[†] Sharon E. Worthington,[‡] Morris Krauss*,[§] and Bernard R. Brooks[||]

Center for Molecular Modeling, Center for Information Technology, National Institutes of Health, Bethesda, Maryland 20892, National Institute of Diabetes & Digestive & Kidney Diseases, National Institutes of Health, Bethesda, Maryland 20892, Center for Advanced Research Biotechnology/National Institute of Standards and Technology, Rockville, Maryland 20850, and Laboratory of Biophysical Chemistry, National Heart Lung and Blood Institute, National Institutes of Health, Bethesda, Maryland 20892

Received: August 29, 2002

The reaction path for the rearrangement of chorismate to prephenate in B.subtilis has been determined in a QM/MM study including the entire protein environment while treating the reaction with ab initio quantum chemistry. In addition to the reactant, chorismate, the side-chains of glu78 and arg90 are included in the quantum region to explore whether the strong ionic hydrogen bonding of the side chains to the substrate has a catalytic effect. The hydrogen bonds from glu78 and arg90 induce electronic effects that activate the substrate. The energetic residue analysis finds that the binding from arg7, arg63, and arg90 are all catalytic due to a differential stabilization along the reaction path of the transition state with respect to the reactant by the local environment. A global QM/MM optimization including the entire protein environment shows only slight changes in the protein environment around the active site along the reaction path. The rearrangement reaction occurs with almost a complete break in the C−O ether bond in chorismate before the C−C bond forms to create prephenate. In this study, the reacting complex forms a hydrogen bond to arg63 that stabilizes the region near the protein surface where the substrate may enter the active site.

1. Introduction

Chorismate is the key branch point intermediate in the shikimate pathway, which is responsible for the synthesis of aromatic amino acids in bacteria, fungi, and higher plants.[1] Chorismate mutase catalyzes the Claisen rearrangement of chorismate to prephenate by more than a million fold.[2] This intramolecular reaction is the first committed step in the biosynthesis of tyrosine and phenylalanine and a rare example of a pericyclic rearrangement catalyzed by an enzyme.[1] This enzyme is of interest not only as a target for the discovery of antibiotics, antifungals, and herbicides but also for understanding enzyme catalytic rate enhancements. In recent years, numerous computational studies have examined this reaction to determine a detailed catalytic mechanism and the roles of the different residues in the enzyme.[3−11] It is well established both experimentally[6,12,13] and theoretically that the enzyme catalyzes this rearrangement by preferentially stabilizing the polar transition state through electrostatic interactions and preferentially binding the pseudodiaxial conformer of the reactant. It is also generally accepted that both the catalyzed and uncatalyzed reactions proceed through a chairlike transition state with the catalyzed transition state being more polar.[14,15] However, there is disagreement on the specific roles of essential catalytic residues as well as details of the structures of both the reactant and transition state bound in the active site.[3−10] The differences can be related to the strong charge and polarization interactions between substrate and enzyme in the very ionic active site. Charge transfer and polarization effects are described accurately by ab initio methods whereas these interactions are not adequately represented in the semiempirical methods, such as AM1. Since ionic hydrogen bonds are a unique feature of enzymatic catalysis, it is essential to model charge transfer and polarization associated with enzymatic catalysis at the ab initio level.

Recently Worthington et al.[16] applied the newly developed effective fragment potential (EFP) method[17] to the Claisen rearrangement of chorismate in B.subtilis chorismate mutase. Their findings support the general contributions of the enzyme to the rate enhancement and also provide new understanding and insight into the enzyme's role due to the charge transfer and polarization. The EFP study shows that glu78 plays an important catalytic role through a charge-transfer interaction with the hydroxyl group on the cyclohexadienyl ring. This interaction, which preactivates the cleaving ether bond through electron delocalization in the cyclohexadienyl ring, is demonstrated to be a significant catalytic interaction of the enzyme. Experimental mutagenesis data also illustrates the catalytic importance of glu78. Even the mutation glu78gln, which can maintain a neutral hydrogen bond to the cyclohexadienyl hydroxide, reduces the specific activity by more than 1000-fold.[18]

Unlike previous studies, the electrostatic stabilization of the transition state by the arg90 residue was not indicated by differences in binding geometry along the reaction path in the EFP study.[16] Rather they make no assignment of this stabilization to a particular residue since all the ionic and polar interactions of the enzyme active site-transition state complex are found to have an effect due to redistribution of charge within the separating fragments. The focus on arg90 in the AM1 studies

[†] Center for Molecular Modeling.
[‡] National Institute of Diabetes & Digestive & Kidney Diseases.
[§] Center for Advanced Research Biotechnology/National Institute of Standards and Technology.
[||] Laboratory of Biophysical Chemistry.

10.1021/jp0268718
Published on Web 10/24/2002

stems from mutagenesis experiments[19] suggesting this residue is essential for the enzyme reaction and also from the perturbation energy shift obtained by removing this residue from the QM/MM calculation.[3] The ab initio QM/MM study can examine the catalytic properties of all the active site residues with an analogous perturbation treatment with the structures in the active site along the reaction path now more accurately determined with ab initio quantum interactions.

The stabilization of the separated fragments in the polar transition state by the highly ionic active site is exhibited in the EFP study by the increased distance between the two fragments of the transition state relative to the in vacuo conformation.[16] On the other hand, the reaction path and transition state using the AM1 quantum potential in a QM/MM study, finds that the enzyme transition state geometry does not change measurably from the in vacuo structure.[9] The transition state structure will now be determined with ab initio quantum interactions in the active site along with the classical interactions of an optimized protein environment.

In the present work the extent to which the enzyme environment varies along the reaction path will be explored. Although the binding of the substrate in the active site involves substantial reorganization in the protein, the assumption has been made that the enzyme environment does not change significantly along the reaction pathway because of the strong ionic interactions between the active site and the substrate. The similarity between the protein environment for the reactant and transition state equilibrium conformation is of fundamental interest and will be directly determined in the present ab initio QM/MM study.

An ab initio QM/MM study is warranted for two important reasons. The most important is that the quantum behavior of the reacting complex will now sense the interaction potential of the entire flexible protein and solvation sphere. The second reason is that all previous QM/MM studies used AM1 quantum potentials with the exception of very limited ab initio QM/MM studies.[5,7] These ab initio studies did not address the changes in the enzyme along the reaction path nor the quantum interactions of the active site residues with the reacting substrate. The AM1 method cannot adequately model charge transfer effects and other electronic properties of the substrate and environment, which are shown in the EFP study to change significantly upon forming the substrate-enzyme complex. Therefore, a new QM/MM study, that treats one or more residues quantum mechanically, is justified.

2. Experimental Method

2.1. Combined Potentials of Quantum Mechanics and Molecular Mechanics. In the present QM/MM method, the substrate and selected active site atoms of the protein are treated quantum mechanically with the GAMESS−US[20] electronic structure code while the bulk of the protein is treated classically using the CHARMM potential.[21]

An interaction potential is applied through a link atom hydrogen to properly interface the two distinct regions. This method has been successfully utilized to model the catalytic mechanism of aldose reductase where multiple hydrogen-bonding interactions occur between substrate and protein.[21] This QM/MM method is now applied to chorismate mutase to both properly represent the reaction path and ensure that this path is responding to the optimized potential for the entire protein environment.

2.2. Docking and Energy Minimization. The coordinates of chorismate mutase complexed with an *endo*-oxabicyclic inhibitor (2cht)[13] were obtained from the Protein Data Bank.[22]

SCHEME 1

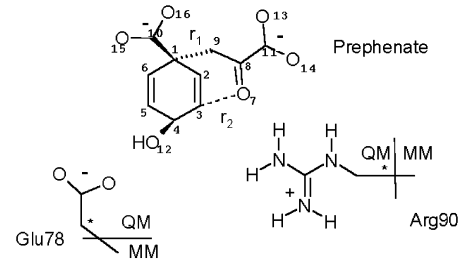

TABLE 1: Comparison of Critical Interactions along Reaction Path between Active Site Residues and Substrate (Å)[a]

	chorismate[b]	transition state QM/MM	prephenate
E78OE2−O12	2.85	2.82	2.87
	1.89	1.85	1.91
cys75NH−O12	2.88	2.83	2.78
	1.88	1.84	1.80
cys75SH−O12	3.45	3.55	3.64
	2.46	2.62	2.74
R7HH12−O13	2.74	2.73	2.75
	1.77	1.75	1.77
R7HH21−O14	2.71	2.70	2.72
	1.73	1.71	1.73
R90HE−O7	2.83	2.81	3.03
	2.06	2.01	2.28
R90HE−O14	2.82	2.86	2.84
	1.95	1.99	1.92
R90HH22−O7	2.83	2.60	2.65
	1.69	1.64	1.68
R63HH12−O16	2.90	2.72	2.71
	1.76	1.76	1.77
Y108OH−O13	2.79	2.80	2.84
	1.84	1.85	1.89

[a] Numbering given in figure attached to table, first line is heavy atom-heavy atom distance and second line is heavy atom-hydrogen distance. [b]

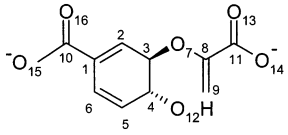

Chorismate with relevant numbering.

Hydrogens were added to the amino acid residues of chorismate mutase with the HBUILD routine of CHARMM.[23] On the basis of the structure of an *endo*-oxabicyclic inhibitor at the active site, the product prephenate was constructed using Quanta 2000. In our computer simulations, the trimer of chorismate mutase has prephenate in each of the three active sites but prephenate is an all-electron molecule only in the A/C active site. Prephenate in the A/B and B/C active sites is treated entirely classically**.** Charge assignments on prephenate and the hydration of the trimer as well as the energy minimization of the hydrated protein complex by CHARMM using an all-atom parameter set[24] were carried out on a cluster of Lobos supercomputers[25] according to the standard procedures published elsewhere.[21]

2.3. QM/MM Partition and Restrained Distance Method. Using the CHARMM energy minimized geometry, the active site of chorismate mutase formed by the A/C domains was partitioned into the QM and MM regions as shown in Scheme 1. Initially, the entire prephenate was described quantum mechanically or all-electron while all other atoms was treated classically. Important binding interactions between the substrate and the active site are given in Table 1 with the active site for prephenate depicted in Figure 1. Prephenate was described using the Hartree−Fock wave function with a 4-31G or double-ζ basis

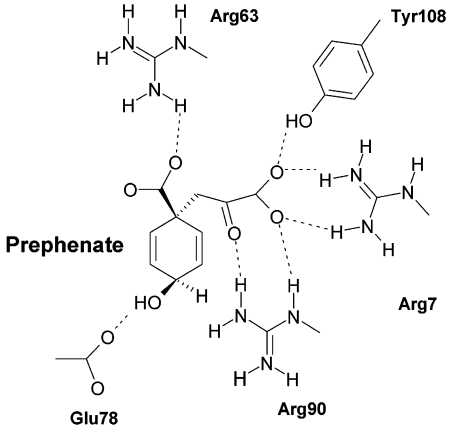

Figure 1. The model of the active site showing the important hydrogen bonding between prephenate and the enzyme residues.

set. No qualitative change is observed in the structure of the ionic active site of a metalloenzyme when polarization functions are added to a double-ζ basis set.[26] With this partition, the geometry of the complex was further minimized using GAMESS/CHARMM with the ad**a**pted basis Newton−Raphson (ABNR) method until the root-mean-square gradient for the last 10 cycles fell to less than 0.05 kcal mol^{-1} Å^{-1}.

After obtaining the QM/MM optimized geometry of prephenate at the active site, the conversion of prephenate to chorismate was investigated by utilizing the restrained distance (RESD) method. RESD is used to restrain a general linear combination of coupled distances to locate a transition state. In this case the selected distances are the breaking ether bond, C3−O7, and the C1−C9 bond formed to create the prephenate product. These coordinates were chosen from the intrinsic reaction coordinate found in the QMEFP calculation.[16] The harmonic restraint term, $E_{res} = {}^{k}/_{2}(r_1 - r_2 - \delta)^2$ was included in the energy minimization processes where k is set to 1500 kcal mol^{-1} Å^{-2}, r_1 and r_2 are the distances C1−C9 and C3−O7, respectively, and δ is a variable parameter, the difference between r_1 and r_2. The forward and reverse reactions were examined by varying δ from −2.0 to 2.0 Å and then back to −2.0 Å, respectively, with an increment of 0.2 Å with two hundred cycles of energy minimization on each grid point. Several scans were required to converge the QM and MM regions with this constraint as shown in Figure 2. The reaction path is described by the bond breaking, C3−O7, and bond making, C1−C9, distances given in Table 2, as well as by the critical hydrogen bonding to the active site residues along the reaction path.

TABLE 2: Comparison of Bond Breaking and Making Distances in Transition State (Å)

	QM/MM (HF)				
	linker 0	linker 1	EFP	in vacuo	QM/MM (AM1)
C3−O7	2.30	2.50	2.35	2.10	1.87
C1−C9	2.50	2.69	2.55	2.45	2.12

After a transition state on the potential energy surface was located, further energy minimizations on the geometry of the reactant, transition state, and product were carried out treating the side chains glu78 and arg90 quantum mechanically with link atoms connecting the QM region to the MM region denoted by the asterisks in Scheme 1. This was done to obtain the full charge transfer and polarization effects of the charged residues on the geometry and energetics of the reactant, transition state, and product.

3. Results and Discussion

3.1. Prephenate Bound to the Active Site. The structure of the product, prephenate, in the active site provides a validation point for this calculation. Although the X-ray structure[13] exists for this complex, it was not used to initiate the calculations. The initial structure for the classical and QM/MM optimization with prephenate in the active site was built from the structure with the transition state analogue.[13] Comparison between the X-ray structure, the QMEFP,[16] and the present QM/MM optimization is made for a range of interactions but focusing on the residues, arg90 and glu78. The binding arrangement of prephenate to enzyme is in good agreement, as seen in Table

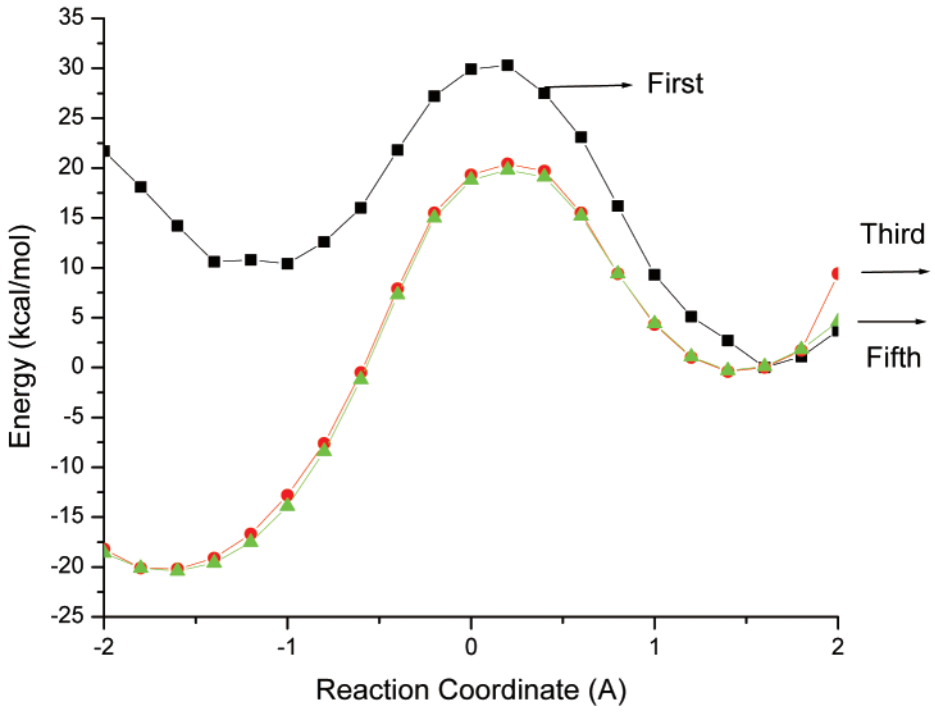

Figure 2. Potential energy surface along the reaction path for the RESD scans leading to convergence.

TABLE 3: Comparison of QM/MM, X-ray, and EFP Structure for the Prephenate Bound in the Active Site (Å)

	QM/MM	X-ray	EFP
E78-O12	2.82	2.70	2.73
Cys75amide	2.79	2.77	3.38
R90HH22−O7	2.65	2.91	3.79
R7HH12−O13	2.75	2.79	2.93

3, for the hydrogen bonding interactions to the hydroxyl group, O12H including the amide of cys75 and the important hydrogen-bonding interaction to OE2 of glu78. The accuracy of the position of prephenate near the glu78 is also reflected in the stacking of the cyclohexadienyl ring with respect to the phenyl ring of phe57 with the calculation agreeing within 0.1 Å of the C−C distances measured for the crystal structure. The binding of arg7 and tyr108 to the carboxylate of the pyruval group is also quite good. The calculated heavy atom bonding distance of arg90 to the pyruval carbonyl is to somewhat shorter distances than the average experimental value[13] with the QM/MM distance indicating a strong hydrogen bond. The QM/MM bond distances are much closer for binding to prephenate than the earlier EFP results.[16] The differences in arg90 binding to the carbonyl oxygen are almost certainly related to the variation in the structure of the different binding sites found in the X-ray structure. For example, the A/B, A/C, and B/C active sites differ in the hydrogen bonding to the O14 carboxylate oxygen in prephenate with values of 2.14, 1.98, and 2.32 Å**,** respectively.

For the QM/MM calculation starting from the A/C site, prephenate binds tightly to arg7, arg63, and arg90. Arg7 binds to the pyruvyl carboxylate with a hydrogen-bond distance of 1.79 Å. Arg63 forms a hydrogen bond with the ring carboxylate with a distance of 2.0 Å, while arg90 hydrogen bonds to the carbonyl oxygen with a distance of 1.68 Å for the calculation with only the substrate treated quantum mechanically and 1.88 Å when glu78 and arg90 are also treated quantum mechanically. Adding the two residues to the quantum region does not change the optimized conformations qualitatively but does produce significant quantitative changes for the hydrogen bonds due to the substantial bond overlap and charge transfer. This is true for all minimized conformations on the reaction path.

The strength of the hydrogen bond from the arg90 to the carbonyl O7 on prephenate is of considerable interest since spectroscopic validation of the structure is possible by comparing calculated with experimental frequencies for the infrared region around the carbonyl stretch frequency.[27] The experimental spectrum finds the frequency is not shifted upon binding to the enzyme suggesting a weak interaction. This is not consistent with the strong binding implied by the short arg90NH22···O7 distance of 1.68 Å or even 1.88 Å with the arg90 treated quantum mechanically. The calculation of the frequency for the prephenate bound in the active site in the EFP structure finds a small vibrational frequency shift (20 cm^{-1}), which is more consistent with the experiment (<5 cm^{-1}). Since the QM/MM bonding is in reasonable agreement with the average experimental distance, this suggests that several local minima are possible, which may lead to differences between the crystal and solution binding structures. The range of hydrogen-binding distances found for the different active sites in the crystal structure support this contention.

3.2. Geometry and Energetics along the Reaction Path. The potential energy, Figure 2, as a function of $(r_1 - r_2 - \delta)$ displays a large decrease in the total energy going from the first scan to the second scan. This is largely due to the relaxation of the protein environment along the all-electron reaction path. This leads to stable values of the MM electrostatic and VDW energy in the last scans as shown in Table 4. The difference between the total energy at each grid point becomes less than one tenth kcal/mol between the fourth and the fifth scan suggesting the system has reached stable stage after the fourth scan. Convergence is also reflected in the energy variation as a function of r_1 and r_2 that are given in Table 4. The variation in the energy along the reaction path is seen to reside almost entirely in the quantum region. The classical region varies much less during the reaction. At the chorismate and prephenate endpoints the VDW energies are essentially equal and the electrostatic energy differs by only 2 kcal/mol.

TABLE 4: Energetic Decomposition of the Classical Component of the Total QM/MM Energy along the Reaction Path (kcal/mol)

reaction pathway	total energy	QM/MM	VDW	ES
−2	−545764.8	−521647.7	−2838.6	−23311.5
−1.8	−545766.3	−521647.1	−2838.6	−23313.1
−1.6	−545766.6	−521645.8	−2838.9	−23314.1
−1.4	−545765.8	−521643.6	−2839.4	−23314.8
−1.2	−545763.7	−521640.4	−2840.3	−23315.2
−1	−545760.1	−521636.2	−2841.1	−23315.5
−0.8	−545754.6	−521630.3	−2841.5	−23315.7
−0.6	−545747.4	−521623.1	−2841.7	−23316.0
−0.4	−545738.9	−521615.2	−2841.4	−23316.1
−0.2	−545731.2	−521609.7	−2840.0	−23315.2
0	−545727.4	−521611.0	−2837.5	−23312.7
0.2	−545726.4	−521611.9	−2836.9	−23311.7
0.4	−545727.1	−521612.0	−2837.8	−23312.0
0.6	−545731.0	−521614.1	−2839.3	−23313.0
0.8	−545736.8	−521619.4	−2839.8	−23313.4
1	−545741.8	−521624.6	−2839.9	−23313.5
1.2	−545745.1	−521628.6	−2839.9	−23313.3
1.4	−545746.5	−521630.9	−2839.8	−23313.0
1.6	−545746.1	−521631.4	−2839.7	−23313.0
1.8	−545744.4	−521630.8	−2839.1	−23313.0
2	−545741.6	−521629.0	−2838.4	−23313.4

The protein environment is very similar along the reaction path from chorismate to transition state. This is shown more directly in Figure 3 by superimposing the protein classical environments of the reactant minimum and the transition state. There is a small reorganization in the binding of arg90 to the ether (carbonyl) and pyruvyl carboxylate oxygens along the reaction path. The binding to the ether or forming carbonyl oxygen is only about 0.05 Å shorter for the hydrogen to O7 distance in the transition state than in the reactant. There is a larger decrease in the heavy atom distance indicative of a more linear hydrogen bond. Even this small shift was not observed in the QMEFP calculation where the distances did not change substantially. An even larger reduction of 0.2 Å in this hydrogen-bonding distance occurs when arg90 is treated quantum mechanically. In the QMEFP calculation, there was no relaxation of the protein environment. On the other hand changes in the internal coordinates of the rearranging substrate do not affect the binding of the carboxylate groups to their respective arginines much since these ionic interactions remain relatively strong and consistent as the substrate reacts.

The activation of the reactant observed in the EFP calculation is also observed here in the substantial increase in the C3−O7 bond distance that will be broken in the rearrangement. The lengthening of the C3−O7 bond is even larger than in the EFP case because of the short hydrogen bond from arg90 to O7. Polarization of the ether bond by this strong hydrogen bond to arg90 now seems the dominant interaction that is activating the ether bond for dissociation. When arg90 is made quantum, the hydrogen bond slightly lengthens from 1.68 to 1.88 Å with the concomitant reduction in the C3−O7 bond from 1.53 to 1.51

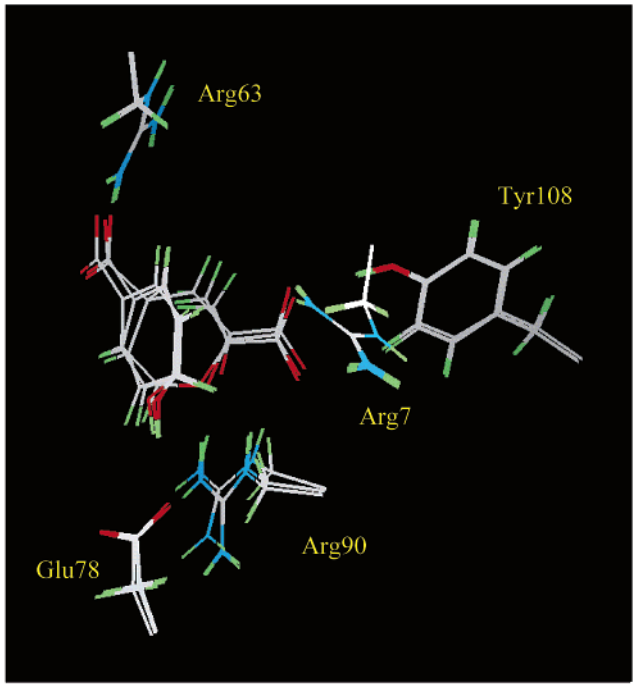

Figure 3. Superimposed structures of the protein environment around the active site binding of the reactant and the transition state.

Å. The lesser role of glu78 is indicated by the observation that the OH bond increases from 0.96 to 0.98 Å when the description of glu78 goes from classical to quantum in the QM/MM calculation but is 0.99 Å in the EFP calculation. The larger separation of the cyclohexadienyl and pyruval fragments in the enzyme relative to the in vacuo transition state is in good agreement with the earlier EFP calculation. The very different behavior for the QM/MM(AM1) is shown in Table 2 as well.

Relative energetics from the fifth scan as tabulated in Table 4 indicates conversion of chorismate to prephenates has an activation energy (E_a) of 19.7 kcal/mol and a reaction enthalpy (ΔH) of −20.5 kcal/mol. The E_a from QM/MM calculations is lower by about 20 kcal/mol from the in vacuo calculation due to the stabilization of the transition state by the surrounding MM charges. The activation energy was further lowered to 16.6 kcal/mol when the side chains Glu78 and Arg90 were treated quantum mechanically.

Figure 4 displays the process of bond-breaking (C3−O7) as well as bond-making (C1−C9) during the conversion of chorismate to prephenate. These processes can be classified into four stages. In the first stage of the reaction, the ether bond, C3−O7, elongates slightly, about 0.2 Å, from 1.49 to 1.69 Å while the C1− C9 distance shortens about 0.66 Å from 3.28 to 2.51 Å. In the second stage that leads up to the transition state, the C3−O7 distance is further elongated to 2.30 Å while the C1−C9 distance remains essentially unchanged, 2.5 Å. In the third stage after passing the transition state, the C3−O7 distance remains constant, 2.3 Å, while the C1−C9 distance is shortened to 1.88 Å. At the last stage, a continuous increase in the C3−O7 distance as well as the formation of the C1−C9 bond can be seen. Overall, the conversion of chorismate to prephenate occurs with the C−O ether bond of chorismate almost completely dissociating before the C−C bond of prephenate is formed.

3.3. Residue by Residue Analysis. The active site of chorismate mutase includes several charged residues that are obviously important in binding the dianionic substrate along the reaction path. To assess whether these interactions have a

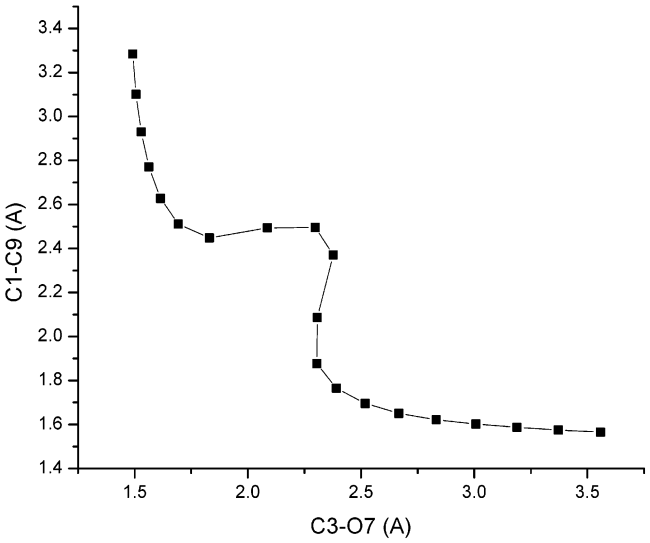

Figure 4. A plot of the variation in the bond lengths of C1−C9 vs C3−O7 showing the complete breaking of the C3−O7 bond before the formation of the C1−C9 bond.

catalytic effect, the residue by residue analysis for the reactant, transition state, and product has been obtained. This analysis calculates the energy difference between a bound complex (e.g., reactant) with the full MM potential and the same complex with zero charge on atoms of a single amino acid residue. The plot of the energy difference vs residue number (Figure 5) provides the electrostatic interaction for each residue of chorismate mutase with that bound ligand. For example, in the complex with the reactant in the active site, turning-off charge on arg90 or on asp118 stabilizes or destabilizes the system by 136.8 kcal/mol and by 142.8 kcal/mol, respectively. Furthermore, a plot of the difference in energy between the reactant and the transition state as a function of residue number (Figure 5c) suggests that arg90, glu78, and arg7 stabilize the transition state while asp118 destabilizes the transition state with the catalytically stabilizing electrostatic effect from arg90 the largest at 9.6 kcal/mol. This supports the earlier theoretical suggestion[3] of the catalytic importance of this residue and is consistent with a number of experimental papers that deduce an important role for arg90.[19] This result is consistent with the shorter hydrogen bond and the differential shortening found from the reactant to the transition state in the QM/MM calculation. The destabilizing influence of asp118 is not supported by the mutation of this residue into asn118 where the rate is actually lowered by a factor of 2.[28] However, this residue is near the end of the C-terminus of the enzyme and the selected mutated species does not have the remaining tail of the C-terminus experimentally or in the theoretical model. The the structures of the C-terminus is poorly defined in the crystal structures,[13] and the structures that are found are different in different active sites suggesting that a molecular dynamics study is required to understand the catalytic behavior of asp118.

Arginine 7 is also indicated to be a catalytic residue. Arg7 acts in concert with arg90 in binding the pyruvyl moiety. It is part of the network of arginines required to bind and stabilize the dianionic substrate. The residue analysis reflects this binding network with arg63 illustrating the balancing of binding for the reactant and the transition state in this network. On the other hand, the apparent destabilizing influence of asp118 emphasizes the importance of charged residues that are not in the first binding shell of the active site. Asp118 is coupled to both arg116 and arg63 on that side of the active site. The strength of the coupling seems to be dependent on which independent crystal

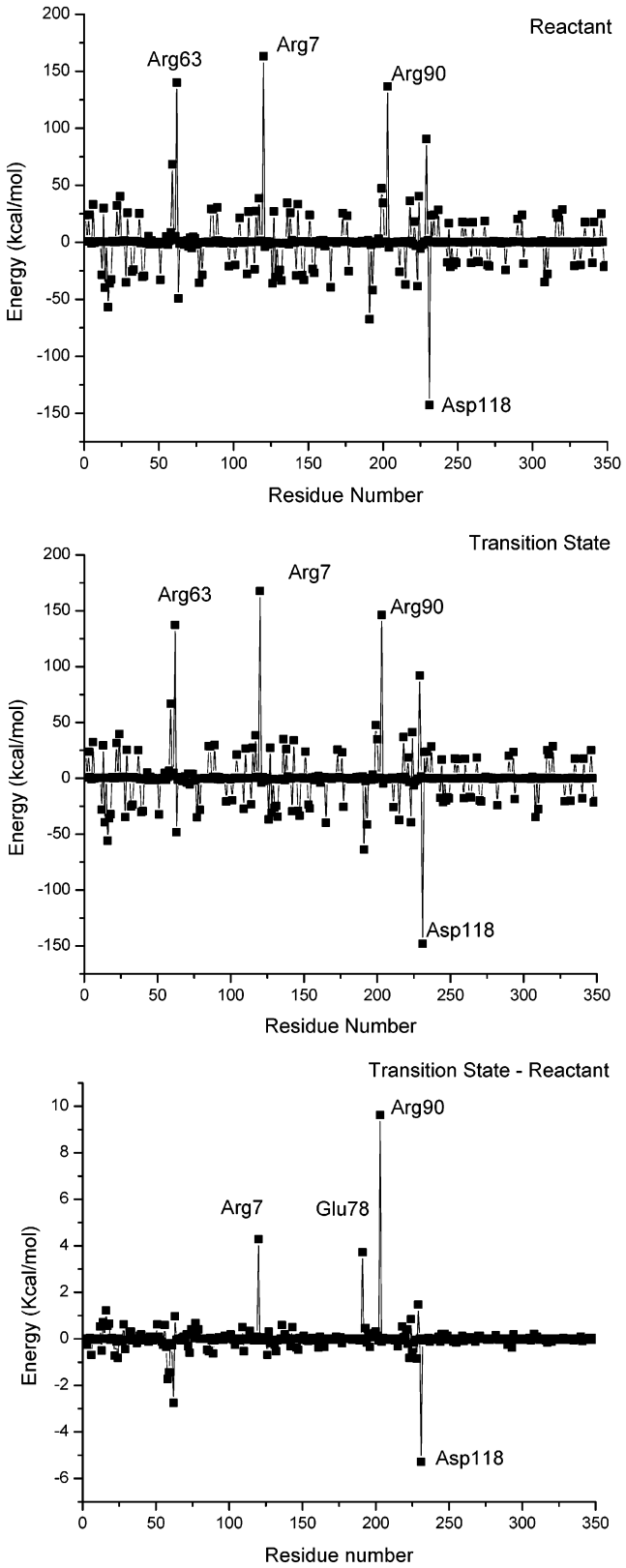

Figure 5. a. The energy contribution by the indicated residue to the binding of the reactant. The active site is constructed from two interacting monomers and the residue numbering scheme is an arbitrary range containing both monomers used in the calculation. b. The energy contribution by the indicated residue to the binding of the transition state. c. The differential or catalytic energy contribution by the indicated residue between the reactant and transition state.

site is chosen to initiate the QM/MM or EFP calculation and an apparent balancing found in the binding between the substrate and the protein residue carboxylates and the arginines.

The Mulliken charges provide a qualitative basis for understanding the charge shifts during the reaction. The charges on the atoms vary slightly except near the rearranging bonds. Even the largest change is only a 10% increase in the charge on O7, which hydrogen bonds to arg90. There is also a modest charge increase on the pyruval C═C bond reflecting a charge redistribution after bond breaking. The primary reason for the catalytic binding effect determined in the residue analysis is the closer bond distance and more directed hydrogen bonding of arg90 to the O7 oxygen carbonyl found in the QM/MM calculation.

4. Conclusion

The findings of this study are summarized as follows: (1) Catalytic residues are deduced from both structural and charge calculations. The importance of the glu78 residue suggested by the QMEFP calculation is confirmed by the QM/MM results but the catalytic importance of arg90 is found to both activate the ether bond and stabilize the transition state as found in the energy residue analysis. The residue analysis also suggests that arg7 is catalytically important suggesting that all the direct ionic interactions to the substrate are catalytically significant in addition to their obvious role in binding. (2) Large polarization and charge-transfer effects are seen in both the reactant and transition state structures, including activation of the ether bond in the reactant, stressing the importance of an ab initio treatment of the all-electron quantum region. The local charge distribution changes at this oxygen suggesting that a structural analysis along the reaction path must be accompanied by an analysis of the charge distribution. However, the main polarizing effect for the transition state is the stabilization by the ionic active site of a large distance between the separating pyruval and cyclohexadienyl fragments. (3) The global QM/MM optimization determines that the protein environment does not change significantly from reactant to transition state. (4) The product complex in the active site is used to validate the QM/MM calculation and shows that a single starting structure can be leveraged into the binding of others along the reaction path or for ligands with comparable charge distribution to the substrates used initially. (5) The charge perturbation residue analysis shows that many, if not all, the charged residues in and near the active site play a catalytic role.

References and Notes

(1) Knaggs, A. R. *Nat. Prod. Rep.* **2001**, *18*, 334−55.
(2) Lee, A. Y.; Stewart, J. D.; Clardy, J.; Ganem, B. *Chem. Biol.* **1995**, *2*, 195−203.
(3) Lyne, P. D.; Mulholland, A. J.; Richards, W. G. *J. Am. Chem. Soc.* **1995**, *117*, 11345−50.
(4) Carlson, H. A.; Jorgensen, W. L. *J. Am. Chem. Soc.* **1996**, *118*, 8475−84.
(5) Davidson, M. M.; Gould, I. R.; Hillier, I. H. *J. Chem. Soc., Perk. Trans. 2* **1996**, *4*, 525−32.
(6) Khanjin, N. A.; Snyder, J. P.; Menger, F. M. *J. Am. Chem. Soc.* **1999**, *121*, 11831−46.
(7) Hall, R. J.; Hindle, S. A.; Burton, N. A.; Hillier, I. H. *J. Comput. Chem.* **2000**, *21*, 1433−41.
(8) Marti, S.; Moliner, A. J.; Silla, E.; Tunon, I. Bertran, J. *Theor. Chem. Acc.* **2001**, *105*, 207−12.
(9) Marti, S.; Andres, J.; Moliner, V.; Silla, E.; Tunon, I.; Bertran, J.; Field, M. J. *J. Am. Chem. Soc.* **2001**, *123*, 1709−12.
(10) Guo, H.; Cui, Q.; Lipscomb, W. N.; Karplus, M. *Proc. Natl. Acad. Sci. U.S.A.* **2001**, *98*, 9032−7.
(11) Hur, S.; Bruice, T.C. *Proc. Natl. Acad. Sci. U.S.A.* **2002**, *99*, 1176−81.
(12) Guilford, W. J.; Copley, S. D.; Knowles, J. R. *J. Am. Chem. Soc.* **1987**, *109*, 5013−19.
(13) Chook, Y. M.; Gray, J. V.; Ke, H.; Lipscomb, W. N. *J. Mol. Biol.* **1994**, *240*, 476−500.

(14) Copley, S. D.; Knowles, J. R. *J. Am. Chem. Soc.* **1985**, *107*, 5306−8.
(15) Gustin, D. J.; Mattei, P.; Kast, P.; Wiest, O.; Lee, L.; Cleland, W. W.; Hilvert, D. *J. Am. Chem. Soc.* **1999**, *121*, 1756−7.
(16) Worthington, S. E.; Roitberg, A. E.; Krauss, M. *J. Phys. Chem. B* **2001**, *105*, 7087−95.
(17) Day, P. N.; Jensen, J. H.; Gordon, M. S.; Webb, S. P.; Stevens, W. J.; Krauss, M.; Garmer, D.; Basch, H.; Cohen, D. *J. Chem. Phys.* **1996**, *105*, 1968−86.
(18) Kast, P.; Hartgerink, J. D.; Asif-Ullah, M.; Hilvert, D. *J. Am. Chem. Soc.* **1996**, *118*, 3069−70.
(19) Kast, P., Asif-Ullah, M., Jiang, N., Hilvert, D. *Proc. Natl. Acad. Sci. U.S.A.* **1996**, *93*, 5043−8.
(20) Schmidt, M. W.; Baldridge, K. K.; Boatz, J. A.; Elbert, S. T.; Gordon, M. S.; Jensen, J. H.; Koseki, S.; Matsunaga, N.; Nguyen, K. A.; Su, S. J.; Windus, T. L.; Dupuis, M.; Montgomery, J. A. *J. Comput.Chem.* **1993**, 1347−63.
(21) Lee, Y. S.; Hodoscek, M.; Brooks, B. R.; Kador, P. F. *Biophys. Chem.* **1998**, *70*, 203−16.
(22) Berman, H. M.; Westbrook, J.; Feng, Z.; Gilliland, G.; Bhat, T.N.; Weissig, H.; Shindyalov, I. N.; Bourne, P. E. *Nucl. Acids Res.* **2000**, *28*, 235−42.
(23) Brooks, B. R.; Bruccoleri, R. E.; Olafson, B. D.; States, D. J.; Swaminathan, S.; Karplus, M. *J. Comput.Chem.* **1983**, *4*, 187−217.
(24) Molecular Simulation, Parameter file for CHARMm, version 22; Waltham: MA, 1992.
(25) Brooks, B. R. 2001. This study utilized the high-performance computational capabilities of the Biowulf/LoBoS3 cluster at the National Institutes of Health, Bethesda, MD.
(26) Krauss, M.; Gilson, H.S. R.; Gresh, N. *J. Phys. Chem.* **2001**, *B105*, 8040−9.
(27) Gray, J. V.; Knowles, J. R. *Biochemistry* **1994**, *33*, 9953−59.
(28) Gamper, M.; Hilvert, D.; Kast, P. *Biochemistry* **2000**, *39*, 14087−94.